

Sidestepping Intermolecular Hydrogen Bonds: How Single Water Molecules Adsorb and Assemble on the Calcite(104)–(2 × 1) Surface

Jonas Heggemann, Jie Huang, Simon Aeschlimann, Simon Spiller, Adam S. Foster,* and Philipp Rahe*



Cite This: *ACS Nano* 2025, 19, 26650–26658



Read Online

ACCESS |

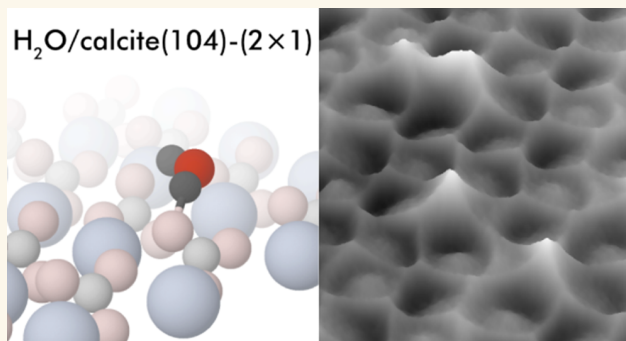
Metrics & More

Article Recommendations

Supporting Information

ABSTRACT: The adsorption of water on mineral surfaces has a decisive impact on processes in the geological, geochemical, biological, and technological contexts. In this work, we investigate the water/calcite(104)–(2 × 1) interface at the single-molecule level by direct imaging with CO-tip-assisted noncontact atomic force microscopy (NC-AFM) and by density functional theory (DFT) calculations combined with NC-AFM image simulations. For single water molecules, the adsorption geometries within the (2 × 1) calcite unit cell are consistently identified by experiments and simulations. The energetic difference between the energetically most favorable adsorption position next to a bulk-like carbonate row (QS water) and the less favorable adsorption geometry next to a reconstructed carbonate row (PR water) can be explained by the local relaxation of the calcite(104) surface nearby a PR water molecule that locally restores the unreconstructed (1 × 1) surface structure. Different combinations of QS and PR water molecules yield a variety of water dimer configurations. We find that the dimer adsorption energy is mostly identical to the sum of the individual molecule energies. From successively raising the sample temperature up to 170 K at half monolayer coverage, we observe that all water molecules move to the most favorable QS position. Overall, the first layer of water molecules on the calcite(104) surface is strongly bound to the substrate in the absence of intermolecular hydrogen bonds.

KEYWORDS: calcite, water, reconstruction, noncontact atomic force microscopy, surface hydration



INTRODUCTION

Key geochemical processes such as the cycling of elements, the storage of carbon dioxide, or the purification of potable water all occur at mineral-water interfaces.¹ Calcite, one of the most abundant minerals in the earth's crust, is particularly relevant in this context as it forms a central constituent in dissolution–precipitation and weathering processes.² Naturally, the hydrated calcite(104) surface has intensively been studied by theoretical and experimental means.^{3–8} While the experimental focus has often been set on *in situ* studies of the fully hydrated surface in liquid environments,^{3–5} theoretical work has addressed in detail both the adsorption of single water molecules^{6–8} and the characteristics of hydration layers.⁹ Until very recently, studies have been based on assuming a (1 × 1) calcite(104) surface geometry, although compelling evidence has recently been given that the pristine calcite(104) surface expresses a (2 × 1)¹⁰ reconstruction¹⁰ that can influence molecular adsorption.^{11,12}

Here, we investigate the water/calcite(104)–(2 × 1) interface at the single molecule level by a combination of high-resolution noncontact atomic force microscopy (NC-AFM) experiments,

density functional theory (DFT) calculations, and NC-AFM image simulations. We identify two different adsorption geometries and thereby clarify the adsorption of single water molecules on the (2 × 1)-reconstructed calcite surface. These geometries appear globally different but are structurally locally similar, yet with an energetic difference of about 0.2 eV. All water molecules diffuse to the low-energy position when approaching thermal equilibrium. From studying the structure and energetics of water dimers, we furthermore do not find evidence for intermolecular hydrogen-bonds within the first water layer. Instead, the water structure is strongly templated by the calcite(104) surface.

Received: April 7, 2025

Revised: June 16, 2025

Accepted: June 18, 2025

Published: July 16, 2025



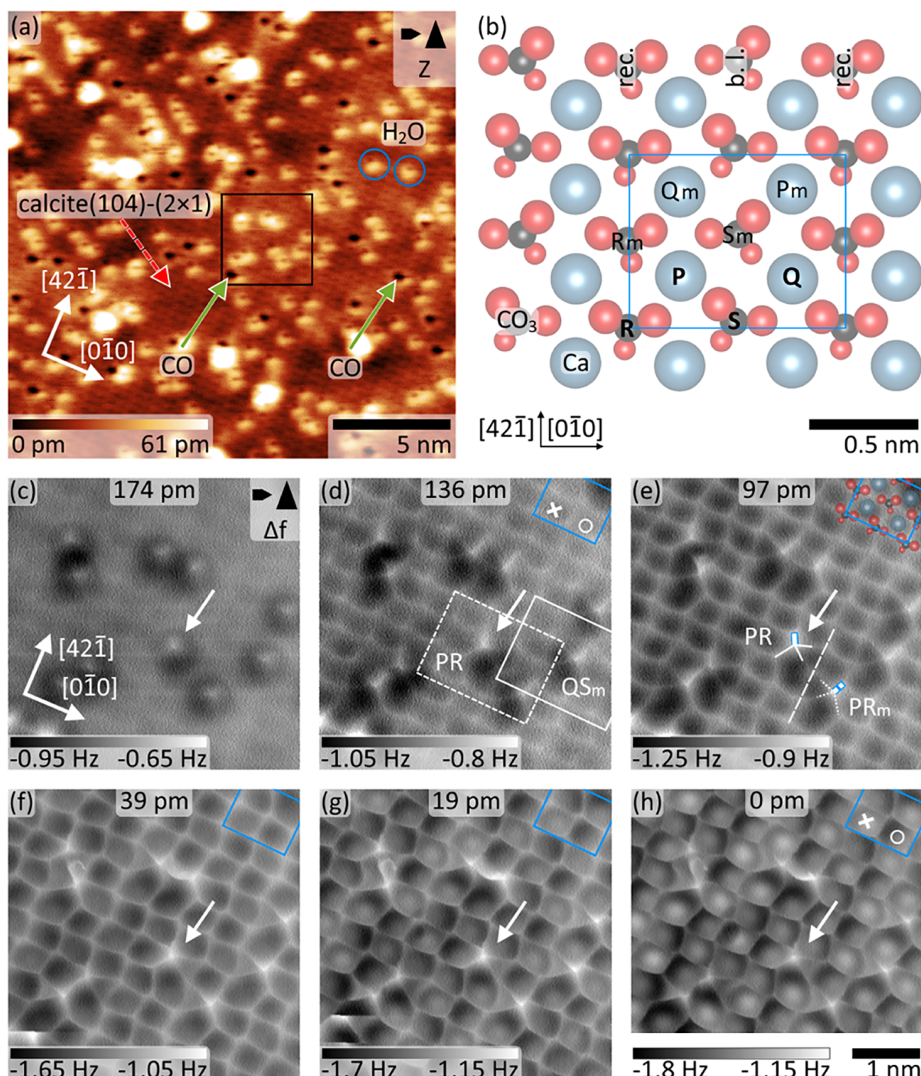


Figure 1. (a) Topography image of a water and CO-covered calcite(104)–(2 × 1) surface acquired with NC-AFM at 5 K ($\Delta f = -0.9$ Hz and $U_{\text{sample}} = 10$ V). Water was deposited in total for 80 s on the sample cooled to 125 K. CO was dosed into the cold scan head for 20 s. Single CO molecules are apparent as dark depressions (two examples marked by green arrows), while single water molecules appear as bright protrusions with a small black spot (two marked by blue circles). (b) Structural model of the (2 × 1)-reconstructed calcite(104) surface.¹⁰ Carbonate groups (calcium atoms) are depicted by red and black (blue) spheres. The rectangular unit cell (blue rectangle) has dimensions of 1 nm × 0.81 nm. The (2 × 1) reconstruction is expressed by a rotation of every second carbonate (CO₃) group along the [010] direction,¹⁰ leading to a reconstructed (rec., R) and bulk-like (b.l., S) row and two calcium sites P and Q. Axes of glide reflection have been found to be located on the carbonate group rows.¹⁰ Consequently, it is convenient to label the symmetry-equivalent carbonate group (calcium) sites in the upper unit cell half by R_m and S_m (P_m and Q_m). (c–h) High-resolution frequency-shift (Δf) images acquired in constant-height mode at the center of panel (a) with a CO-terminated tip. The height is decreased before acquisition of each image with the relative position indicated at the top. (Experimental parameter figure c–h: $U_{\text{tip}} = 10$ V. Vertical stability ensured by active drift compensation.¹³)

RESULTS AND DISCUSSION

NC-AFM topography image data (see Figure 1a) acquired at 5 K present an overview over the water and carbon monoxide (CO)-covered calcite(104)–(2 × 1) surface, representative for a calcite(104) sample after deposition of submonolayer coverage of water on a cooled sample and dosing of CO directly into the cold scan head. Three characteristic features are identified in this image: (i) the calcite surface lattice with atomic resolution (one exemplary area marked by a dashed red arrow), (ii) single CO molecules apparent as dark depressions with a bright rim¹⁰ (two examples marked by green solid arrows), and (iii) single water molecules imaged as bright features with a small depression (two examples marked by blue circles).

The pristine calcite(104) surface expresses a (2 × 1) reconstruction with a rectangular unit cell of size 1 nm × 0.81 nm, containing four calcium ions and four carbonate (CO₃) groups in the top layer; the DFT-optimized structural model is shown in Figure 1b.¹⁰ Within the (2 × 1) surface unit cell, four specific sites can be defined¹⁰ as shown in Figure 1b: two carbonate group sites and two calcium ion sites. The (2 × 1) reconstruction mainly modifies every second carbonate group row along the [010] direction; one exemplary group is marked by “R” in Figure 1b. Compared to the bulk-like carbonate group (marked by “S” in Figure 1b), which basically remains in the bulk-like geometry, the reconstructed carbonate group is rotated such that the top oxygen atoms are located on roughly the same vertical height. Correspondingly, two calcium ion positions are

present which we herein denote by "P" and "Q" as marked in Figure 1b. Furthermore, the surface belongs to the planar space group pg that includes a glide-plane symmetry. As a consequence of this surface symmetry property, the four sites R_m , S_m , P_m , and Q_m in the upper unit cell half are the glide-reflected analogons of the four sites R, S, P, and Q with otherwise identical physical properties. Therefore, it is sufficient to discuss one set of the glide-plane related sites when investigating molecular adsorption, i.e., discussing the sites within the lower unit cell half. Further details regarding the surface structure are given in ref 10.

Adsorption Properties of Single Water Molecules. By building upon the recent success in submolecular imaging^{14,15} and atomic-scale mineral surface studies,^{10,16,17} we here study water adsorption in detail with high-resolution NC-AFM imaging. Constant-height frequency shift (Δf) data acquired with a CO-terminated tip at the central area in Figure 1a (marked by a black rectangle) and measured at different tip–sample distances quantified by the tip position z_{tip} ¹⁸ are reproduced in Figure 1c–h. A tip–sample distance range of about 170 pm is sampled (lowest image coordinate arbitrarily set to $z_{\text{tip}} = 0$ pm, relative separations are carefully checked by comparison to $\Delta f(z_{\text{tip}})$ data, see Supporting Information). In these image data, the appearance of the calcite(104)–(2 × 1) surface is identical to previous observations:¹⁰ the protruding oxygen atoms of the surface carbonate groups appear as bright repulsive features, connected by bright linkers, and the calcium atoms are at the center of the dark pores within this lattice. Furthermore, the checkerboard-like appearance at the Ca sites is clearly apparent and the distance-dependent switch of the bright/dark pores is reproduced (the same pore positions are marked by white crosses and circles in Figure 1d,h). This allows us to superimpose the structural DFT model in Figure 1e and include the respective (2 × 1) unit cell outline as a blue rectangle in Figure 1d–h. The positioning of the unit cell vertices on the carbonate group centers (see also Figure 1b) follows the previous convention that is rooted in finding the glide reflection axes to be located on the carbonate group rows.¹⁰

Single water molecules (one example marked by white arrows in Figure 1c–h) within this data set express a very consistent imaging pattern. Generally, we identify a single water molecule at large tip–sample distances (Figure 1c) as a repulsive ("bright") feature with an asymmetric attractive ("dark") surrounding. This pattern is in agreement with the topography-mode images (see Figure 1): a more repulsive interaction with the water molecule leads to a closer approach of the tip at the water center. When moving the constant-height imaging plane toward the surface, four sharp filaments linking the water molecule with the calcite lattice emerge, see also the sketch included in Figure 1e. We find that these linking filaments grow in sharpness, but otherwise remain at identical positions when further reducing the tip–sample distance. One of these filaments (illustrated by a thick white line with blue contour in Figure 1e) is apparent at all tip–sample distances and will be denoted "ridge" throughout this work.

The filament pattern representing a single water molecule is found to exist with two orientations as indicated by the two sketches (drawn by solid and dashed lines) in Figure 1e. From an analysis of their position relative to the calcite (104)–(2 × 1) lattice, it becomes clear that they are related by a glide-plane reflection (axis of glide reflection included as a dashed line in Figure 1e), in agreement with the existence of the glide plane symmetry element within the calcite(104)–(2 × 1) surface geometry.¹⁰ Therefore, their physical properties are identical as

given by symmetry and we instead now focus on the adsorption at the two different sites within the (2 × 1) unit cell.

We have previously conducted an extensive search for the optimum adsorption geometry for a single water molecule on the reconstructed calcite(104)–(2 × 1) surface using DFT,¹² whereby the water adsorption energy E_{water} has been calculated from the difference

$$E_{\text{water}} = E_{\text{total}} - E_{\text{slab}} - E_{\text{single}} \quad (1)$$

between the total energy E_{total} of the combined water/calcite system and the energy E_{slab} (E_{single}) of the calcite slab (of a single gas phase water molecule).

The energetically most favorable configuration has been found with an adsorption energy of $E_{\text{QS}} = -0.98$ V and with the geometry shown in Figure 2a.¹² This adsorption geometry is

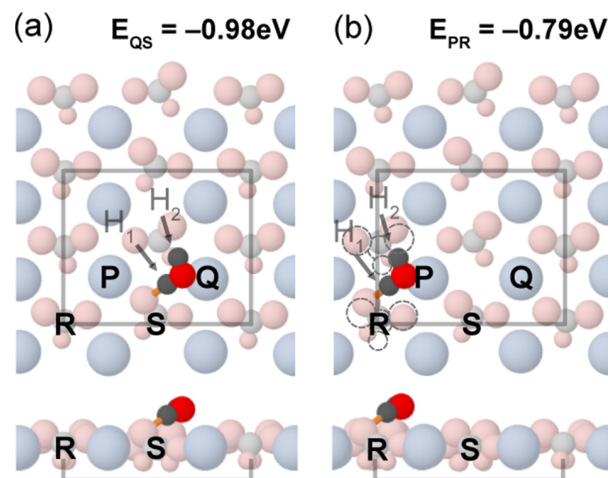


Figure 2. DFT models for (a) a single QS¹² and (b) a single PR water molecule adsorbed on the reconstructed surface. Side views are given in the bottom panels. Hydrogen atoms of the water molecule are indicated by H_1 and H_2 . Outline of the reconstructed carbonate groups next to the PR water are included as dashed circles in (b), see Supporting Information for atomic shifts.

stabilized by an ionic bond between the water oxygen atom (O_{water}) and a surface calcium atom (Ca_{surf}) at site Q as well as by a hydrogen bond (indicated by an orange line) between water hydrogen atom 1 (H_1) and the protruding oxygen atom (O_{surf}) of the adjacent (bulk-like or unreconstructed) carbonate group at site S. Due to this binding situation, this adsorption configuration is denoted as QS water. We calculate bond lengths of 2.4 Å ($O_{\text{water}}-Ca_{\text{surf}}$), 1.8 Å (H_1-O_{surf}), and 2.19 Å (H_2-O_{surf}). This adsorption geometry is in excellent agreement with previous, theoretical literature findings for water adsorption on the unreconstructed calcite(104)–(1 × 1) surface.^{6,7,19,20} In particular, previous DFT studies^{6,7,19} determined a $Ca_{\text{surf}}-O_{\text{water}}$ bond length of about 2.4 Å, while the hydrogen bond has been found to express a $O_{\text{surf}}-H_1$ distance around 1.7 Å. The second $O_{\text{surf}}-H_2$ distance has previously been found^{19,20} to be between 2.3 Å and 2.4 Å. Although the $O_{\text{surf}}-H_2$ distance in our model is slightly shorter than the literature results, it is still too long for a hydrogen bond. Therefore, we understand that the second oxygen–hydrogen bond has mostly a weak dispersive character.

We found a general tendency of the water oxygen atom to bind to a calcium surface ion in our DFT calculations, which we directly understand from the electronegativity of the water oxygen atom. This allows us to identify the calcium P site as a

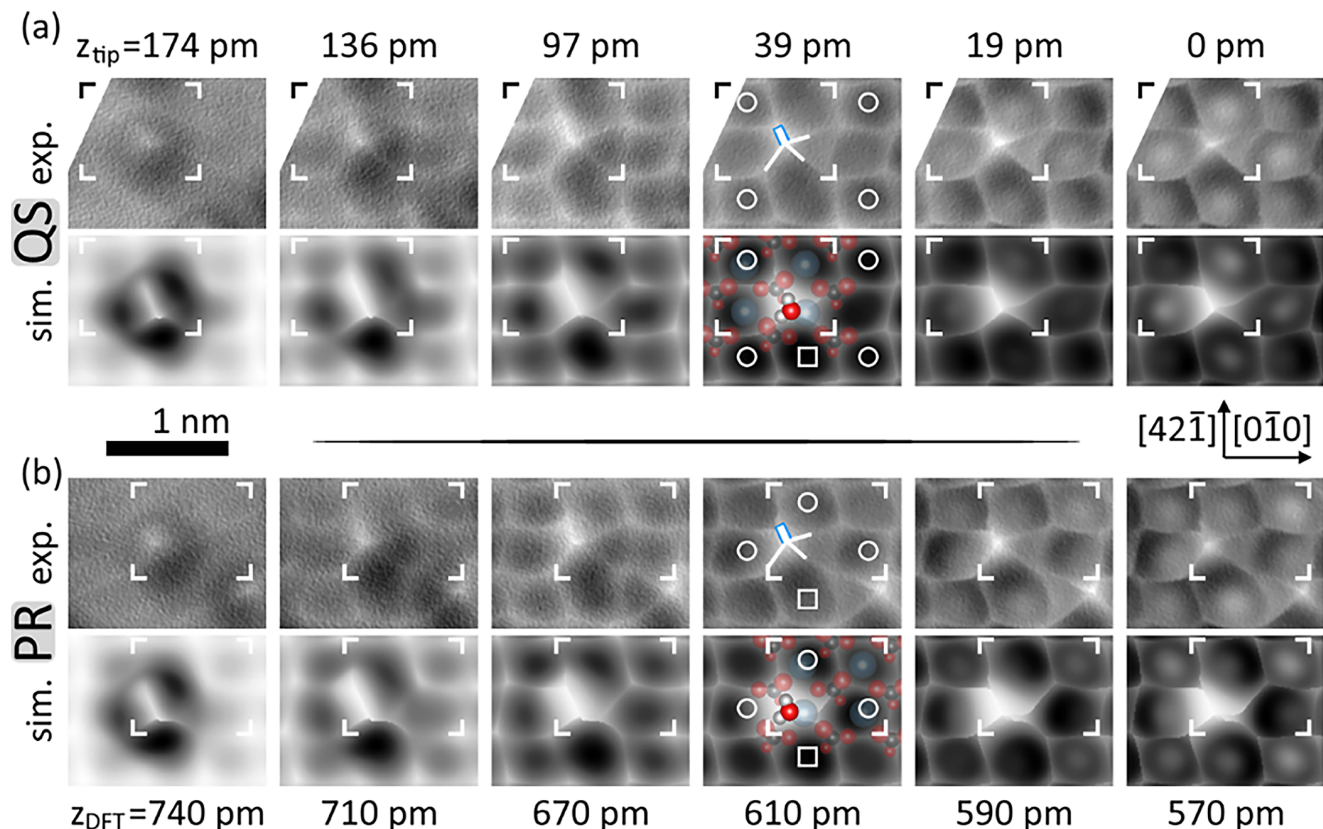


Figure 3. (a) QS water. Experimental results (top row) and simulated images (bottom row) at six tip–sample distances (experimental positions z_{tip} at the top, simulation positions z_{DFT} at the bottom). (b) PR water, experimental results (top row) and simulated images (bottom row). The (2×1) unit cell is marked in all images and the Q calcium sites (dark pores at small tip–sample distances) are marked by white circles in the $z_{\text{tip}} = 39 \text{ pm}/z_{\text{DFT}} = 610 \text{ pm}$ images. Experimental parameters are identical to Figure 1c–h. Experimental data are extracted from the extended image series in Figure 1 at the position of the solid rectangle for the QS water (data are reflected) and dashed rectangle for the PR water. $[42\bar{1}]$ is pointing up in all cases. ($U_{\text{sample}} = 10 \text{ V}$).

possible second water adsorption position within the (2×1) unit cell. Among the water/calcite(104) structures with an oxygen binding to the P-site calcium ion, the geometry of the model with the lowest binding energy of $E_{\text{PR}} = -0.79 \text{ eV}$, denoted as PR water, is shown in Figure 2b. The bond lengths $\text{O}_{\text{water}}-\text{Ca}_{\text{surf}}$ (2.42 \AA) and $\text{H}_1-\text{O}_{\text{surf}}$ (1.87 \AA) of this configuration are only slightly elongated when compared to the QS water geometry. Instead, the difference of the adsorption energy to the QS geometry is explained by the significant modification of the R carbonate groups adjacent to the water molecule (dashed outlines of the reconstructed carbonate groups in absence of water are included in Figure 2b; see Supporting Information for atomic shifts). As is apparent from Figure 2b, this modification brings the calcite surface structure locally close to that of the unreconstructed surface—a clear difference to the QS water geometry, where only minor shifts within the surface layer are found.¹²

Very recently, NC-AFM experiments performed at 140 K revealed that water exclusively adsorbs at the QS sites at coverage up to 0.5 monolayer (ML) and that the adsorption energy per water is reduced at coverage between 0.5 ML and 1 ML.^{11,12} As water is herein deposited on a cooled sample and the system is imaged at 5 K, the PR–QS transition is kinetically limited and both the QS and PR water adsorption geometries can be observed. As the main difference between QS and PR water lies in the positioning of the water molecule relative to the calcite lattice, we use this criterion to extract in Figure 3 one

representative case for each water type from Figure 1 at the areas marked by white rectangles in Figure 1d.

First, the QS adsorption geometry is investigated with experimental data reproduced in the row “exp.” in Figure 3a. The numbers given at the top of each image denote the vertical tip position z_{tip} identical to Figure 1. Image data in the row “sim.” in Figure 3a are simulation results using the probe particle model (PPM)²¹ for the optimum QS geometry that was previously shown in Figure 2a. PPM data are generated using the two-atom flexible CO tip-apex configuration with a flexible oxygen and carbon atom as well as two Cu atoms resembling the tip apex, see ref. 10 for further details. PPM data are presented for six different tip–sample distances (given at the bottom of the figure) with absolute distances z_{DFT} defined as the vertical distance between the Cu tip atom position relative to the average calcium surface plane. The agreement between the experimental and simulated NC-AFM image data is overall excellent when using an offset of 570 pm between the experimental z_{tip} and simulation z_{DFT} axes: At large tip–sample distances, the QS water molecule is imaged as one repulsive feature with a dark rim. Upon reducing the tip–sample distance, the contrast of the before-identified ridge becomes stronger and the water fine structure develops together with the calcite lattice structure. From the structure overlay in the $z_{\text{DFT}} = 610 \text{ pm}$ image, we find that the ridge is located at the $\text{H}_2-\text{O}_{\text{surf}}$ bond position, which was previously identified as a bond with a weak dispersive character. The (2×1) reconstruction is clearly visible in form of the checkerboard

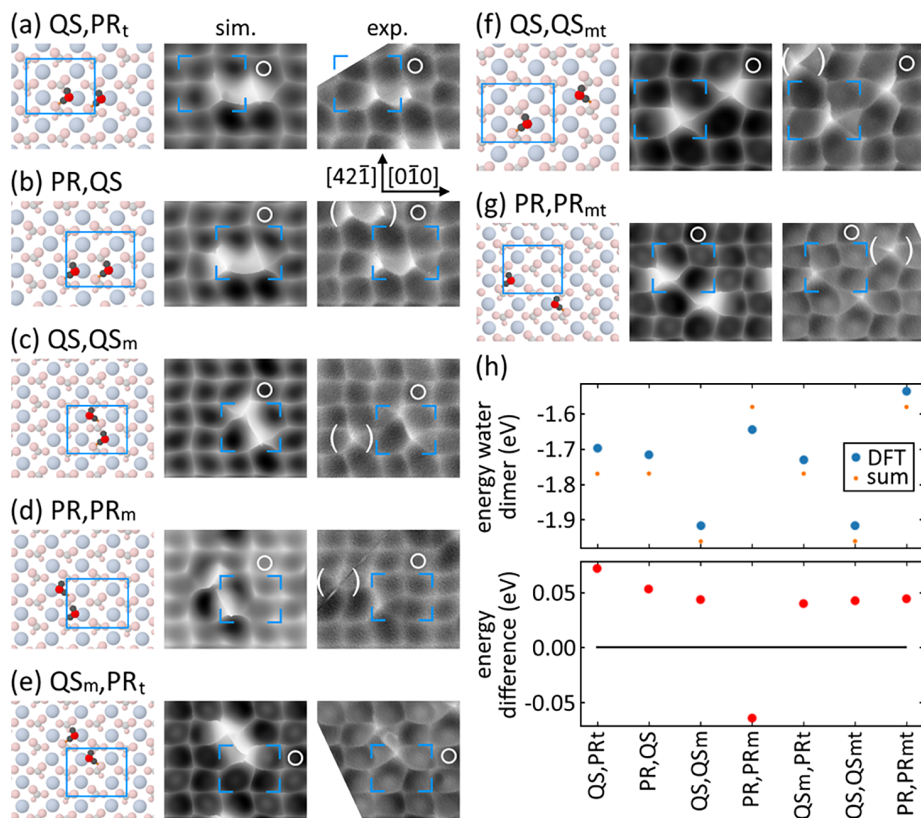


Figure 4. Water dimer structures on calcite(104)–(2 × 1). (a,b) Water dimers formed along the [0̄10] direction. (c–e) Water dimers formed along the [42̄1] direction. (f,g) Water dimers with water molecules separated by one carbonate group row. Left column: DFT-optimized model. Centre column: NC-AFM image simulations using the DFT-optimized model. Right column: Experimental constant-height frequency shift data of the corresponding dimer. Unit cell and Q calcium sites (dark pores at small tip–sample distances) are highlighted by corner markers and circles, respectively. (h, upper panel) Dimer formation energies and sum of individual adsorption energies. (h, lower panel) Energy difference $E_{\text{dimer,DFT}} - E_{\text{dimer,sum}}$ for each dimer. (b,c,d,f,g) White parentheses are added to mark coincidentally present water molecules which are not part of the respective dimer structure. (Experimental parameters: (a,b,f) $U_{\text{sample}} = -3 \text{ V}$; (c) $U_{\text{sample}} = 4.5 \text{ V}$; (d) $U_{\text{sample}} = 4 \text{ V}$; (e,g) $U_{\text{sample}} = 10 \text{ V}$).

pattern: the dark pores at the calcium Q sites are marked in the $z_{\text{DFT}} = 610 \text{ pm}$ image by white circles. From these markers it is clear that the QS water molecule is located at an off-center position within a dark pore. We note in passing that one adjacent calcium site (marked by a white rectangle) is imaged dark as a result of the water-CO tip interaction.

Second, the same analysis is performed for PR water in Figure 3b. The key difference to the previous QS case is the position of the water molecule relative to the calcite surface pattern: From the Q-site markers (white circles) in the $z_{\text{DFT}} = 610 \text{ pm}$ image it is clear that the water molecule is located nearby the “bright” (P) calcium position within the (2 × 1) unit cell, i.e., shifted by half unit cell length along [0̄10] compared to QS water. A comparison via line profiles to further highlight the match between experiment and simulation is included in the Supporting Information. Apart from this difference, the image pattern is virtually identical between the QS and PR case: The ridge and the fine structure develop in similar ways and one adjacent Ca site (marked by a rectangle in the $z_{\text{DFT}} = 610 \text{ pm}$ image) expresses a dark contrast. This close similarity of the QS and PR water patterns can directly be explained by a physical argument: The calcite(104) surface species directly adjacent to the PR water molecule reorient toward the calcite bulk structure, thus the local substrate geometry of a QS water is closely resembled. These data give further strong evidence for the reconstruction lifting mechanism from direct imaging of single

water molecules. As a consequence, the distinction between the QS and PR water geometries in image data is only reliable from comparing the global environment, i.e., from the water positioning relative to the (2 × 1) lattice, as the local environment is virtually identical.

Water Dimer Structures. To investigate the interaction between single water molecules—direct and surface mediated—in the first adsorption layer on the calcite(104)–(2 × 1) surface, we study water dimers. As a consequence of the (2 × 1) reconstruction and *pg* symmetry, a number of different configurations are possible using single QS and PR water molecules. Seven representative cases are shown in Figure 4a–g. For all cases, we present the DFT-optimized dimer model (left column), PPM images simulated for the respective geometries (center column), and experimental data (right column). The image data are extracted from several distance-dependent image series available from simulation and experiment, see Supporting Information. The dimers are named according to their composition by QS- and PR-type water. To further distinguish between the different cases, we add the letter *m* to the single water model name if the water is located at a glide-plane reflected position (i.e., in the upper unit cell half) and the letter *t* in case the water has been translated to an equivalent position outside the central (2 × 1) unit cell. The representative cases can roughly be divided by water molecules arranged along the [0̄10] direction (Figure 4a,b), by water positioned along the [42̄1]

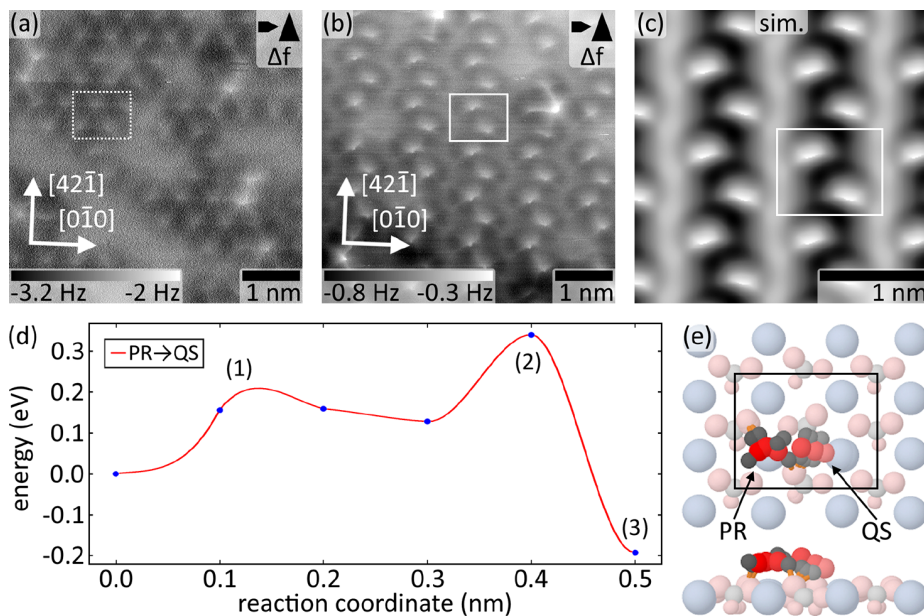


Figure 5. (a) Water assembly after deposition of about 0.3 ± 0.1 ML onto a sample held at about 125 K. (b) QS row formation after temporarily annealing the sample to about 170 K (experimental parameters: (a) $U_{\text{sample}} = 2$ V; (b) $U_{\text{sample}} = 1$ V). (c) PPM image simulation of a QS water row structure (DFT model from ref 12). The (2×1) unit cell is marked by a white rectangle in all images. (d) NEB calculation for the transition between the PR and QS geometry. (e) Superposition of the geometries of the NEB calculation.

direction (Figure 4c–e), as well as by water molecules that are separated by one carbonate group row (Figure 4f,g). In all cases, an excellent match between the simulated and experimental data is achieved as the fine structure is precisely reproduced. The distinction between the QS and PR cases again relies on analyzing the water placement relative to the calcite lattice as the surface reconstruction is locally lifted and, therefore, the local water geometry is rather similar.

The corresponding energies required for the water dimer formation as determined from the DFT calculations are reproduced by blue points in Figure 4h. Energies are calculated using eq 1 by setting $E_{\text{water}} \rightarrow 2E_{\text{water}}$. The results are compared to the sum of the respective individual energies E_{QS} and E_{PR} for the single QS and PR water adsorption geometries. Due to the calcite(104)– (2×1) surface symmetry, two energy values are sufficient to also describe the respective glide-reflected (*m*) and translated (*t*) variants of a single water molecule. The energy difference $E_{\text{dimer,DFT}} - E_{\text{dimer,sum}}$ between these energies is shown in the lower panel of Figure 4h. In all cases besides PR/PRm, the positive energy difference highlights a small repulsive contribution with an energy of about 50 meV accompanying the dimer formation. Thus, we do not find evidence for a water–water attraction as would be expected for hydrogen bonding between the water molecules. This is in full agreement with the comparably large distance between the water oxygen and hydrogen atoms. Instead, the small repulsive contribution appears to be substrate mediated. By comparing the atomic positions between the pristine calcite surface and different water models as well as between the single water models and water dimer structures (see Supporting Information), an influence on several adjacent Ca ions and CO_3 groups nearby the water molecules is found. In case of the water dimers, this leads to competing forces that cause an overall small repulsive interaction. Also for the PR/PRm case we do not find water–water attraction, but rather explain the energy gain by the reconstruction lifting mechanism: For a second PR water

molecule adsorbed directly adjacent to a first PR water along the $[42\bar{1}]$ direction, the local surface reconstruction is already partly lifted and, therefore, the adsorption energy of the next water molecule is decreased.¹²

Transition between PR and QS Water. In order to investigate the transition from the PR to the QS water configuration, we perform annealing experiments and nudged elastic band (NEB) calculations. A structure consisting of both PR and QS molecules as presented in Figure 5a is representative for deposition of about 0.3 ± 0.1 ML at a sample held at about 125 K. Apparently, this structure is kinetically limited as temporarily raising the temperature to about 170 K leads to the formation of rows, see Figure 5b. No movement was apparent at temperatures up to 143 K. The comparison in Figure 5c with the PPM simulation for a 0.5 ML water structure exclusively consisting of QS molecules¹² yields an excellent agreement with the experimental data (see Supporting Information for comparison at further tip–sample distances) and confirms the interpretation of previous TPD data.¹¹ Three main steps are identified in NEB calculations during the PR–QS transition, see Figure 5d,e, namely (1) first the cleavage of the $\text{H}_1-\text{O}_{\text{surf}}$ bond (at $r \sim 0.1$ nm) including the reorientation of the adjacent surface carbonate groups (energy cost of less than 0.2 eV). (2) Second, the $\text{O}_{\text{water}}-\text{Ca}_{\text{surf}}$ bond is broken (at $r \sim 0.4$ nm) posing a barrier of about 0.2 eV. (3) Third, reforming the bonds at the QS position yields more than 0.5 eV, leading to an overall gain of 0.2 eV in energy.

CONCLUSIONS

In conclusion, we identified two adsorption geometries of water on the calcite(104)– (2×1) surface at 5 K that have an energetic difference of about 0.2 eV. This analysis is based on high-resolution atomic force microscopy experiments with CO-functionalized tips, density functional theory calculations, as well as NC-AFM image simulations. While the energetically most stable adsorption geometry (QS) corresponds to a water

molecule binding to an unreconstructed carbonate group row, the energetic difference to the second geometry (PR) where water binds to a reconstructed carbonate group row is caused by locally lifting the (2 × 1) reconstruction of the calcite(104) surface at this position.

The analysis of water dimer geometries further confirm the strong influence of the surface, including the (2 × 1) reconstruction, on water adsorption and highlights a small surface-mediated repulsion between most dimer models. Upon driving the system at 0.5 ML toward thermal equilibrium by annealing to 170 K, QS water is exclusively found. In stark contrast to many other water/surface systems, water on calcite(104) does not form a hydrogen-bonded ice-like layer at coverage up to one monolayer, but the assembly is instead templated by the surface.

METHODS

Sample Preparation. A double sample holder²² supporting both a Ag(111)/mica sample for tip preparation and characterization as well as a calcite crystal for high-resolution measurements is used throughout the experiments. Before preparing the samples, the sample holder was heated to about 380 °C for about 90 min.

First, the Ag(111) metal sample surface is prepared by five sputtering (Ar^+ at about 2.2×10^{-6} mbar, 15 min, yielding a drain current of about 2 μA) and annealing (about 380 °C for 15 min) cycles.^{23,24} Second, a clean calcite(104) surface is prepared by cleaving the crystal in vacuum with a sharp blade.²⁵ To reduce charges on the calcite surface that prevent stable NC-AFM measurements, the sample is heated to a temperature of about 160°C for about 1 h.^{26,27}

H₂O Deposition on the Calcite(104) Surface. Water is deposited by dosing (at about 1×10^{-9} mbar) ultrapure H₂O (Millipore water for molecular Biology) into the preparation chamber from a variable leak valve onto a sample cooled to about 125 K. Previous to these experiments, water is cleaned by more than 20 freeze–pump–thaw cycles.

CO Dosing. CO is deposited on the sample by dosing into the cold scan head for 20 s from backfilling the recipient with CO to a recipient pressure of about 5×10^{-8} mbar. The local pressure inside the scan head is expected to be lower, explaining the observation of less than 0.1 ML CO, while the parameters would result in a dosage of 0.75 L.

NC-AFM Experiments. Data are acquired at 5 K with a ScientaOmicron qPlus LT gen.III AFM/STM instrument operated by a MATRIX controller. Piezoelectric qPlus sensors with W tips²⁸ are used as provided by the manufacturer. Sharp tips are prepared on the metal surface by common STM tip preparation strategies. CO is transferred to the tip by vertical manipulation. The CO tip quality is checked from reverse imaging of surface-bound CO molecules. A bias voltage is applied during imaging to compensate for long-range electrostatic forces.

DFT and NEB Calculations. All first-principles calculations in this work are performed using the periodic plane-wave basis VASP code^{29,30} implementing the spin-polarized Density Functional Theory. To accurately include van der Waals interactions for this system, we further use the Tkatchenko-Scheffler method with iterative Hirshfeld partitioning³¹ shown to be best suited for ionic systems.^{32,33} Projected augmented wave potentials are used to describe the core electrons³⁴ with a kinetic energy cutoff of 500 eV (with PREC = accurate). Systematic k-point convergence is checked for all systems with sampling chosen according to the system size. This approach converged the total energy of all the systems to the order of 1 meV. For calculations of the calcite surface, we use a $4 \times 4 \times 4$ supercell (320 atoms total), a vacuum gap of at least 1.5 nm, and a $5 \times 5 \times 1$ k-point grid. The upper two layers of calcite are allowed to relax to a force of less than 0.01 eV/Å. Barrier calculations are performed initially using the standard Nudged Elastic Band (NEB) method with increasing image density³⁵ before implementing the Climbing NEB approach³⁶ to find the final barrier. For these calculations, only the gamma point is used. Energy differences refer to comparisons between equivalent supercells.

NC-AFM Image Simulations. The probe particle model (PPM)^{21,37,38} is used for simulating the high-resolution AFM images, using the two-atom flexible CO tip-apex configuration, consisting of two (fixed) Cu atoms and a flexible carbon and oxygen atom to model the carbon monoxide molecule. Further details can be found in the Supporting Information of ref 10. The parameters of the tip geometry, its stiffness values, and electrostatic properties are fitted by simulating interactions over a pentacene molecule, using DFT.³⁹ The electrostatic interactions between atoms of the tip and sample are taken into account using the Hartree potential of the surface and water molecules above. For the remaining interactions, the Lennard-Jones equilibrium distance parameters are fitted for each individual atom of the topmost layer of CaCO₃ and the water molecules above using a recent probe-particle-model fitting procedure, as used on other ionic systems.^{40,41} Note that the tip-bound CO is allowed to fully relax within the PPM while the surface atoms and the adsorbed water molecules are constrained. This is the most probable explanation for any small differences between the simulated and experimental images.

ASSOCIATED CONTENT

SI Supporting Information

The Supporting Information is available free of charge at <https://pubs.acs.org/doi/10.1021/acsnano.5c05845>.

CIF files for water monomer and dimer models (ZIP)

An explanation of finding the relative position of the experimental data, constant-height imaging of water dimers, constant-height imaging of QS-water row structure, line profiles from single water images, and atomic shifts (PDF)

AUTHOR INFORMATION

Corresponding Authors

Adam S. Foster – Department of Applied Physics, Aalto University, Espoo 00076, Finland; Nano Life Science Institute (WPI-NanoLSI), Kanazawa University, Kanazawa 920-1192, Japan;  orcid.org/0000-0001-5371-5905; Email: adam.foster@aalto.fi

Philipp Rahe – Institut für Physik, Universität Osnabrück, Osnabrück 49076, Germany;  orcid.org/0000-0002-2768-8381; Email: prah@uni-osnabrueck.de

Authors

Jonas Heggemann – Institut für Physik, Universität Osnabrück, Osnabrück 49076, Germany

Jie Huang – Department of Applied Physics, Aalto University, Espoo 00076, Finland;  orcid.org/0000-0003-3560-283X

Simon Aeschlimann – Physical Chemistry I, Faculty of Chemistry, Bielefeld University, Bielefeld 33615, Germany

Simon Spiller – Institut für Physik, Universität Osnabrück, Osnabrück 49076, Germany

Complete contact information is available at:

<https://pubs.acs.org/10.1021/acsnano.5c05845>

Author Contributions

J. Heggemann performed the experiments and analyzed the experimental data. S.A. and S.S. contributed to data acquisition and analysis. J. Huang and A.S.F. performed the calculations. P.R. conceived the project, supported the experiments, contributed to data analysis, and wrote the first manuscript draft. All authors discussed the results and contributed to finalizing the manuscript.

Notes

The authors declare no competing financial interest.

ACKNOWLEDGMENTS

We wish to thank O. Krejčí for support with PPM simulations. Funded by the Deutsche Forschungsgemeinschaft (DFG, German Research Foundation)—289665220, 508007945, and 508008230. Financial support from the Universität Osnabrück via the Innovationspool is gratefully acknowledged. Computing resources from the Aalto Science-IT project and CSC, Helsinki, and funding from the Academy of Finland (project nos. 347319 and 346824) are gratefully acknowledged.

REFERENCES

- (1) Putnis, C. V.; Ruiz-Agudo, E. The Mineral-Water Interface: Where Minerals React with the Environment. *Elements* **2013**, *9*, 177–182.
- (2) Deer, W. A.; Howie, R. A.; Zussman, J. *An introduction to the rock-forming minerals*; Mineralogical Society of Great Britain and Ireland, 2013.
- (3) Teng, H. H.; Dove, P. M.; Orme, C. A.; De Yoreo, J. J. Thermodynamics of calcite growth: baseline for understanding biomineral formation. *Science* **1998**, *282*, 724–727.
- (4) Laanait, N.; Callaghen, E. B. R.; Zhang, Z.; Sturchio, N. C.; Lee, S. S.; Fenter, P. X-ray-driven reaction front dynamics at calcite-water interfaces. *Science* **2015**, *349*, 1330–1334.
- (5) Söngen, H.; Reischl, B.; Miyata, K.; Bechstein, R.; Raiteri, P.; Rohl, A. L.; Gale, J. D.; Fukuma, T.; Kühnle, A. Resolving Point Defects in the Hydration Structure of Calcite (10.4) with Three-Dimensional Atomic Force Microscopy. *Phys. Rev. Lett.* **2018**, *120*, 116101.
- (6) Ataman, E.; Andersson, M. P.; Ceccato, M.; Bovet, N.; Stipp, S. L. S. Functional Group Adsorption on Calcite: I. Oxygen Containing and Nonpolar Organic Molecules. *J. Phys. Chem. C* **2016**, *120*, 16586–16596.
- (7) Lardge, J. S.; Duffy, D. M.; Gillan, M. J. Investigation of the Interaction of Water with the Calcite (10.4) Surface Using Ab Initio Simulation. *J. Phys. Chem. C* **2009**, *113*, 7207–7212.
- (8) de Leeuw, N. H.; Parker, S. C. Atomistic simulation of the effect of molecular adsorption of water on the surface structure and energies of calcite surfaces. *J. Chem. Soc., Faraday Trans.* **1997**, *93*, 467–475.
- (9) Reischl, B.; Raiteri, P.; Gale, J. D.; Rohl, A. L. Atomistic Simulation of Atomic Force Microscopy Imaging of Hydration Layers on Calcite, Dolomite, and Magnesite Surfaces. *J. Phys. Chem. C* **2019**, *123*, 14985–14992.
- (10) Heggemann, J.; Ranawat, Y. S.; Krejčí, O.; Foster, A. S.; Rahe, P. Differences in Molecular Adsorption Emanating from the (2 × 1) Reconstruction of Calcite(104). *J. Phys. Chem. Lett.* **2023**, *14*, 1983–1989.
- (11) Dickbreder, T.; Lautner, D.; Köhler, A.; Klausfering, L.; Bechstein, R.; Kühnle, A. How water desorbs from calcite. *Phys. Chem. Chem. Phys.* **2023**, *25*, 12694–12701.
- (12) Heggemann, J.; Aeschlimann, S.; Dickbreder, T.; Ranawat, Y. S.; Bechstein, R.; Kühnle, A.; Foster, A. S.; Rahe, P. Water adsorption lifts the (2 × 1) reconstruction of calcite(104). *Phys. Chem. Chem. Phys.* **2024**, *26*, 21365.
- (13) Rahe, P.; Schütte, J.; Schniederberend, W.; Reichling, M.; Abe, M.; Sugimoto, Y.; Kühnle, A. Flexible drift-compensation system for precise 3D force mapping in severe drift environments. *Rev. Sci. Instrum.* **2011**, *82* (6), 063704.
- (14) de Oteyza, D. G.; Gorman, P.; Chen, Y.-C.; Wickenburg, S.; Riss, A.; Mowbray, D. J.; Etkin, G.; Pedramrazi, Z.; Tsai, H.-Z.; Rubio, A.; Crommie, M. F.; Fischer, F. R. Direct Imaging of Covalent Bond Structure in Single-Molecule Chemical Reactions. *Science* **2013**, *340*, 1434–1437.
- (15) Gross, L.; Mohn, F.; Moll, N.; Meyer, G.; Ebel, R.; Abdel-Mageed, W. M.; Jaspar, M. Organic structure determination using atomic-resolution scanning probe microscopy. *Nat. Chem.* **2010**, *2*, 821–825.
- (16) Setvín, M.; Reticcioli, M.; Poelzleitner, F.; Hulva, J.; Schmid, M.; Boatner, L. A.; Franchini, C.; Diebold, U. Polarity compensation mechanisms on the perovskite surface $\text{KTaO}_3(001)$. *Science* **2018**, *359*, 572–575.
- (17) Franceschi, G.; Kocán, P.; Conti, A.; Brandstetter, S.; Balajka, J.; Sokolovic, I.; Valtiner, M.; Mittendorfer, F.; Schmid, M.; Setvín, M.; et al. Resolving the intrinsic short-range ordering of K^+ ions on cleaved muscovite mica. *Nat. Commun.* **2023**, *14* (1), 208.
- (18) Rahe, P.; Heile, D.; Olbrich, R.; Reichling, M. Quantitative dynamic force microscopy with inclined tip oscillation. *Beilstein J. Nanotechnol.* **2022**, *13*, 610–619.
- (19) Kerisit, S.; Parker, S. C.; Harding, J. H. Atomistic simulation of the dissociative adsorption of water on calcite surfaces. *J. Phys. Chem. B* **2003**, *107*, 7676–7682.
- (20) Wright, K.; Cygan, R. T.; Slater, B. Structure of the (1014) surfaces of calcite, dolomite and magnesite under wet and dry conditions. *Phys. Chem. Chem. Phys.* **2001**, *3*, 839–844.
- (21) Hapala, P.; Kichin, G.; Wagner, C.; Tautz, F. S.; Temirov, R.; Jelínek, P. Mechanism of high-resolution STM/AFM imaging with functionalized tips. *Phys. Rev. B* **2014**, *90*, 085421.
- (22) Heggemann, J.; Laflör, L.; Rahe, P. Double sample holder for efficient high-resolution studies of an insulator and a metal surface. *Rev. Sci. Instrum.* **2021**, *92* (5), 053705.
- (23) Rusponi, S.; Boragno, C.; Valbusa, U. Ripple structure on $\text{Ag}(110)$ surface induced by ion sputtering. *Phys. Rev. Lett.* **1997**, *78*, 2795–2798.
- (24) Costantini, G.; Rusponi, S.; de Mongeot, F. B.; Boragno, C.; Valbusa, U. Periodic structures induced by normal-incidence sputtering on $\text{Ag}(110)$ and $\text{Ag}(001)$: flux and temperature dependence. *J. Phys.: Condens. Matter* **2001**, *13* (26), 5875.
- (25) Tröger, L.; Schütte, J.; Ostendorf, F.; Kühnle, A.; Reichling, M. Concept for support and cleavage of brittle crystals. *Rev. Sci. Instrum.* **2009**, *80* (6), 063703.
- (26) Wollbrandt, J.; Linke, E.; Brückner, U. Untersuchung elektrostatischer Aufladungen auf Spaltflächen von Alkalihalogenideinkristallen. *Exp. Tech. Phys.* **1975**, *23* (1), 65–73.
- (27) Barth, C.; Henry, C. R. Kelvin probe force microscopy on surfaces of UHV cleaved ionic crystals. *Nanotechnology* **2006**, *17* (7), S155–161.
- (28) Giessibl, F. J. The qPlus sensor, a powerful core for the atomic force microscope. *Rev. Sci. Instrum.* **2019**, *90* (1), 011101.
- (29) Kresse, G.; Furthmüller, J. Efficiency of ab-initio total energy calculations for metals and semiconductors using a plane-wave basis set. *Comput. Mater. Sci.* **1996**, *6*, 15.
- (30) Kresse, G.; Furthmüller, J. Efficient iterative schemes for ab initio total-energy calculations using a plane-wave basis set. *Phys. Rev. B* **1996**, *54*, 11169–11186.
- (31) Tkatchenko, A.; Scheffler, M. Accurate Molecular Van Der Waals Interactions from Ground-State Electron Density and Free-Atom Reference Data. *Phys. Rev. Lett.* **2009**, *102*, 073005.
- (32) Bučko, T.; Lebègue, S.; Hafner, J.; Ángyán, J. G. Improved Density Dependent Correction for the Description of London Dispersion Forces. *J. Chem. Theory Comput.* **2013**, *9*, 4293–4299.
- (33) Bučko, T.; Lebègue, S.; Ángyán, J. G.; Hafner, J. Extending the applicability of the Tkatchenko-Scheffler dispersion correction via iterative Hirshfeld partitioning. *J. Chem. Phys.* **2014**, *141* (3), 034114.
- (34) Blöchl, P. E. Projector augmented-wave method. *Phys. Rev. B* **1994**, *50*, 17953–17979.
- (35) Mills, G.; Jónsson, H.; Schenter, G. K. Reversible work transition state theory: application to dissociative adsorption of hydrogen. *Surf. Sci.* **1995**, *324*, 305–337.
- (36) Henkelman, G.; Uberuaga, B. P.; Jónsson, H. A climbing image nudged elastic band method for finding saddle points and minimum energy paths. *J. Chem. Phys.* **2000**, *113*, 9901.
- (37) Hapala, P.; Temirov, R.; Tautz, F. S.; Jelínek, P. Origin of High-Resolution IETS-STM Images of Organic Molecules with Functionalized Tips. *Phys. Rev. Lett.* **2014**, *113*, 226101.
- (38) Oinonen, N.; Yakutovich, A. V.; Gallardo, A.; Ondráček, M.; Hapala, P.; Krejčí, O. Advancing scanning probe microscopy simulations: A decade of development in probe-particle models. *Comput. Phys. Commun.* **2024**, *305*, 109341.

- (39) Di Giovannantonio, M.; Urgel, J. I.; Beser, U.; Yakutovich, A. V.; Wilhelm, J.; Pignedoli, C. A.; Ruffieux, P.; Narita, A.; Müllen, K.; Fasel, R. On-Surface Synthesis of Indenofluorene Polymers by Oxidative Five-Membered Ring Formation. *J. Am. Chem. Soc.* **2018**, *140*, 3532–3536.
- (40) Peng, J.; Cao, D.; He, Z.; Guo, J.; Hapala, P.; Ma, R.; Cheng, B.; Chen, J.; Xie, W. J.; Li, X.-Z.; Jelínek, P.; Xu, L.-M.; Gao, Y. Q.; Wang, E.-G.; Jiang, Y. The effect of hydration number on the interfacial transport of sodium ions. *Nature* **2018**, *557*, 701–705.
- (41) Liebig, A.; Hapala, P.; Weymouth, A. J.; Giessibl, F. J. Quantifying the evolution of atomic interaction of a complex surface with a functionalized atomic force microscopy tip. *Sci. Rep.* **2020**, *10* (1), 14104.

CAS INSIGHTS™

EXPLORE THE INNOVATIONS SHAPING TOMORROW

Discover the latest scientific research and trends with CAS Insights. Subscribe for email updates on new articles, reports, and webinars at the intersection of science and innovation.

[Subscribe today](#)

CAS
A division of the
American Chemical Society

Supporting Information: Sidestepping Intermolecular Hydrogen Bonds: How Single Water Molecules Adsorb and Assemble on the Calcite(104)–(2 × 1) Surface

Jonas Heggemann,¹ Jie Huang,² Simon Aeschlimann,³
Simon Spiller,¹ Adam S. Foster,^{2,4} and Philipp Rahe¹

¹*Institut für Physik, Universität Osnabrück,
Barbarastraße 7, 49076 Osnabrück, Germany*

²*Department of Applied Physics, Aalto University, Espoo 00076, Finland*

³*Physical Chemistry I, Faculty of Chemistry, Bielefeld University,
Universitätsstraße 25, Bielefeld 33615, Germany*

⁴*Nano Life Science Institute (WPI-NanoLSI),
Kanazawa University, Kanazawa 920-1192, Japan*

I. RELATIVE POSITION OF EXPERIMENTAL DATA

The relative height positions of the experimental data in the main manuscript Figs. 1 and 3 are determined from a comparison between $\Delta f(z_p)$ -curves and the Δf values extracted from the experimental image data. This evaluation consists of three steps.

First, two $\Delta f(z_p)$ -curves are acquired at each of the three positions (A, B, and C) marked in the constant-height image in Fig. S1(a). In this image, the calcite lattice is clearly visible. The scanned area is identical to the area in main text Fig. 1(c-h) with a small lateral shift due to thermal drift. Care was taken to only using positions for the $\Delta f(z_p)$ -curves where a small lateral deviation is not expected to result in appreciable different $\Delta f(z_p)$ data. Therefore, two dark pores and one linker are chosen. The two curves for each position are averaged to reduce noise and to now serve as a vertical scale (Fig. S1(b)).

Second, to determine the relative height positions, the Δf -values are extracted at the respective positions A, B, and C from each image of the image series, and translated via the $\Delta f(z_p)$ -curves into a height information. To highlight this procedure using main text Fig. 1(c): The frequency shift value at position C is read from the image to be -0.82 Hz . Then, using the blue $\Delta f(z_p)$ -curve acquired at position C in Fig. S1(b) allows to determine the acquisition height of this position along the curve axis at about 142 pm (light green arrows).

In the third step, the three height values (Fig. S1(c)) of each of the eight images are averaged (green stars) and fitted by a linear function (red line). This line has a slope of $(-18.8 \pm 0.6)\text{ pm image}^{-1}$, hence, the images have a relative height difference of about -19 pm . With this difference of -19 pm it is also possible to assign image heights to images with Δf values lower than the values of the $\Delta f(z_p)$ -curves (here -1.47 Hz) as required for panels g and h of main text Fig. 1.

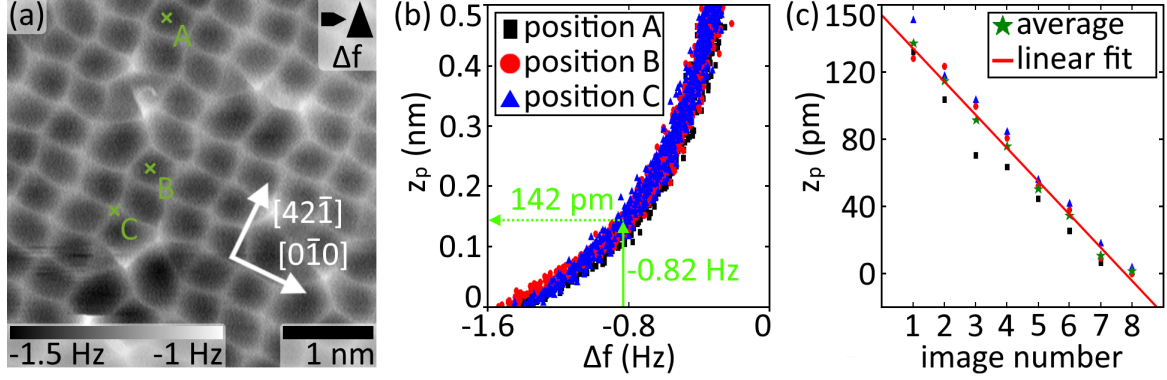


FIG. S1. (a) High-resolution frequency-shift (Δf) image acquired in constant-height mode with a CO-terminated tip showing the same sample area as in main text Fig. 1(c-h). A small lateral shift is present due to thermal drift ($U_{tip} = 10$ V). Two $\Delta f(z_p)$ -curves were measured at each of the three positions marked by green crosses. Two curves are averaged at each position with the results shown in (b). (c) The estimated image heights of eight constant-height images derived from the three $\Delta f(z_p)$ -curves for each position. The green stars indicate the average height for each image and the red line is a linear fit with a slope of (-18.8 ± 0.6) pm image $^{-1}$.

II. CONSTANT-HEIGHT IMAGING OF WATER DIMERS

High-resolution NC-AFM images for water dimers are extracted from series of constant-height images acquired at different height. Fig. S2 to Fig. S8 each present the experimental image series (right column) complemented by the simulated data (left column) for seven different dimer types.

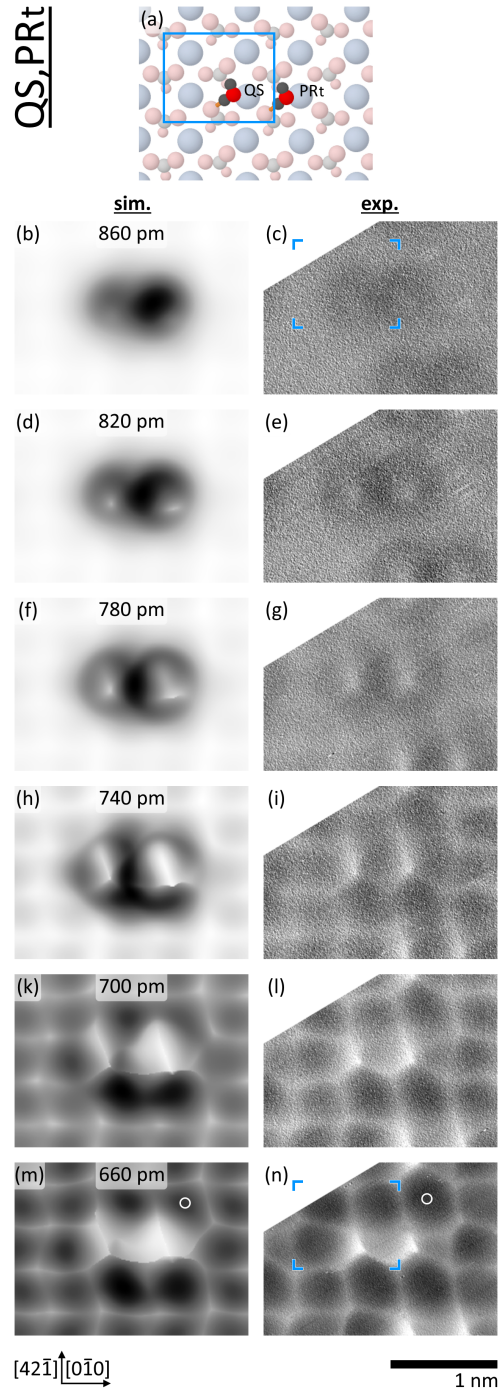


FIG. S2. QS,PRt dimer: (a) DFT model as well as (b,d,f,h,k,m) simulated and (c,e,g,i,l,n) experimental constant-height frequency shift images.

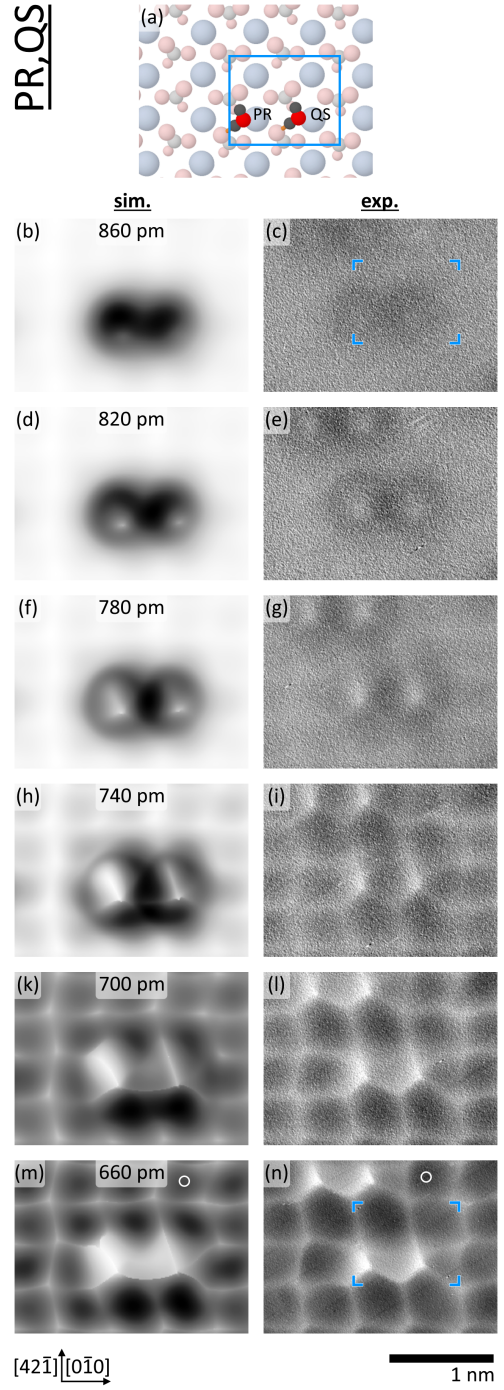


FIG. S3. PR,QS dimer: (a) DFT model as well as (b,d,f,h,k,m) simulated and (c,e,g,i,l,n) experimental constant-height frequency shift images.

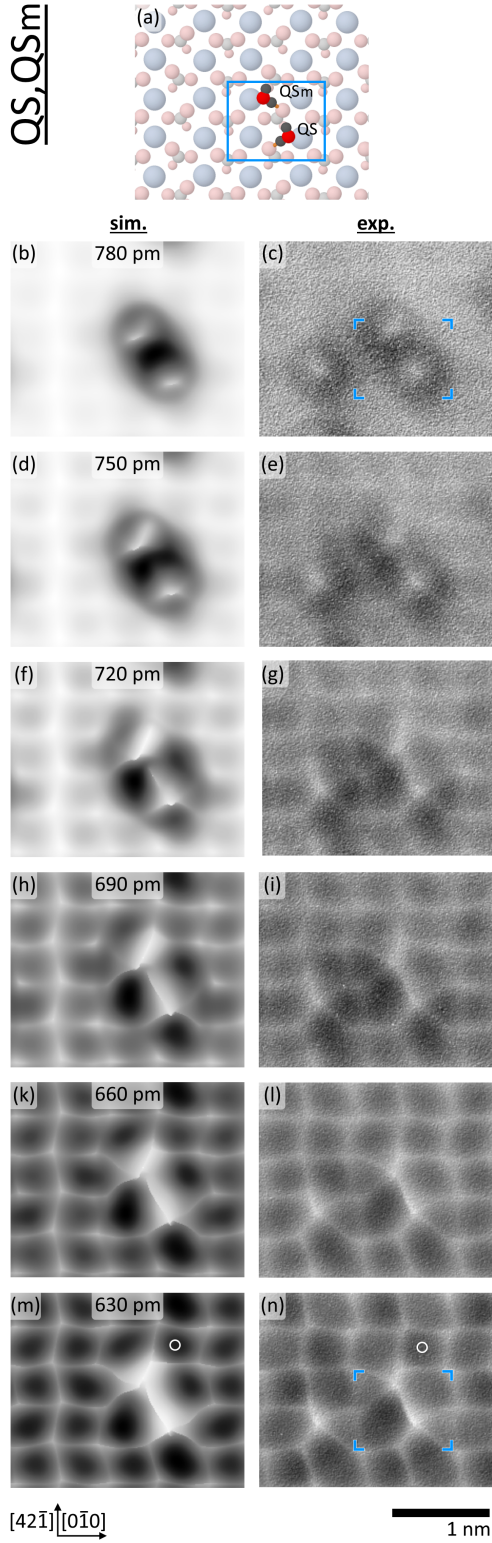


FIG. S4. QS, QSm dimer: (a) DFT model as well as (b,d,f,h,k,m) simulated and (c,e,g,i,l,n) experimental constant-height frequency shift images.

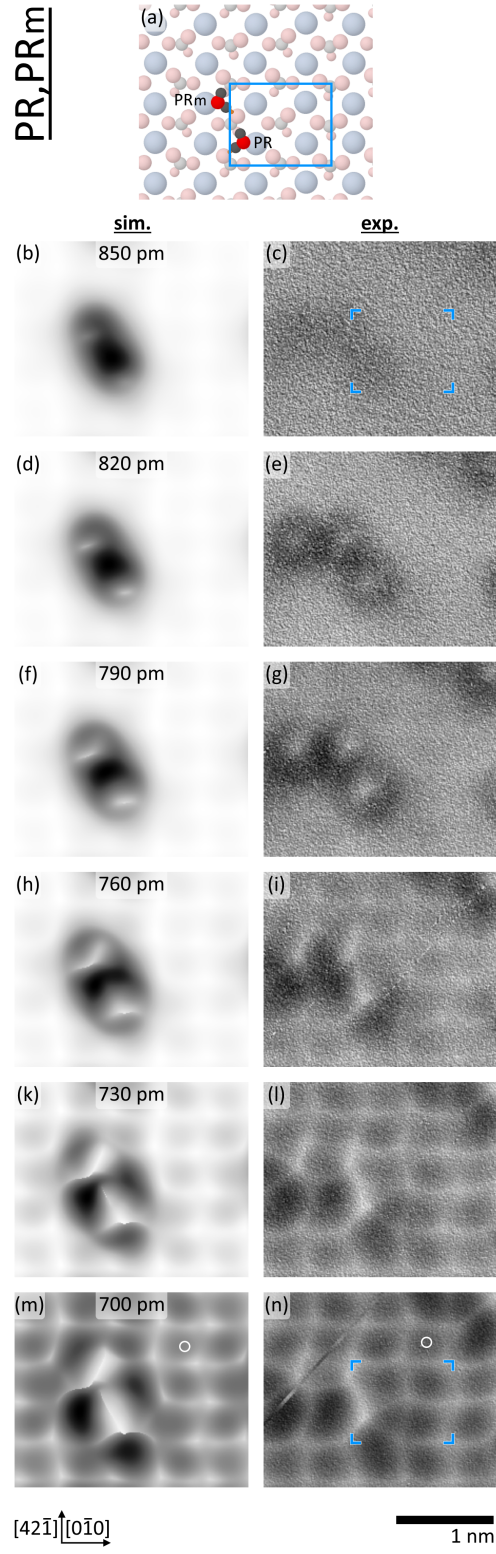


FIG. S5. PR,PRm dimer: (a) DFT model as well as (b,d,f,h,k,m) simulated and (c,e,g,i,l,n) experimental constant-height frequency shift images.

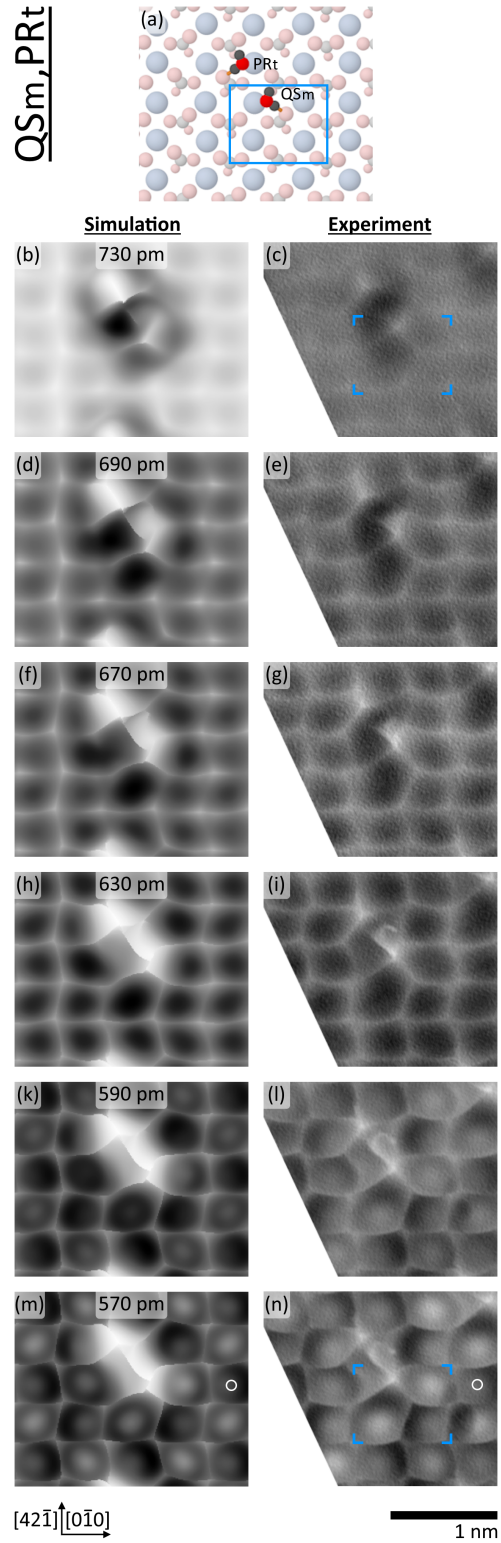


FIG. S6. QSm,PRt dimer: (a) DFT model as well as (b,d,f,h,k,m) simulated and (c,e,g,i,l,n) experimental constant-height frequency shift images.

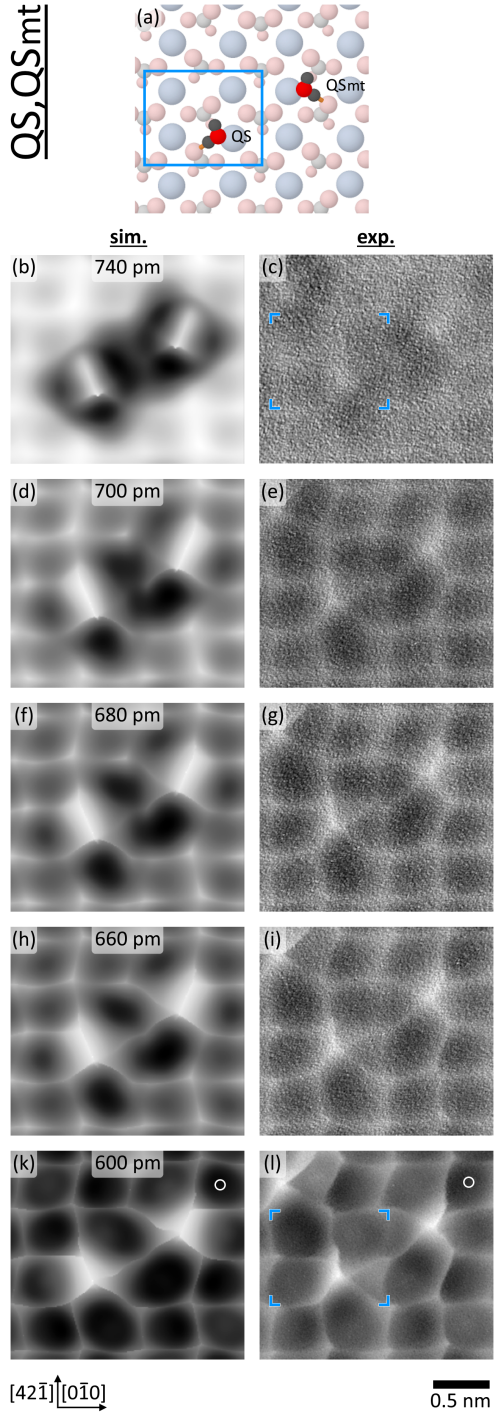


FIG. S7. QS,QSmt dimer: (a) DFT model as well as (b,d,f,h,k) simulated and (c,e,g,i,l) experimental constant-height frequency shift images.

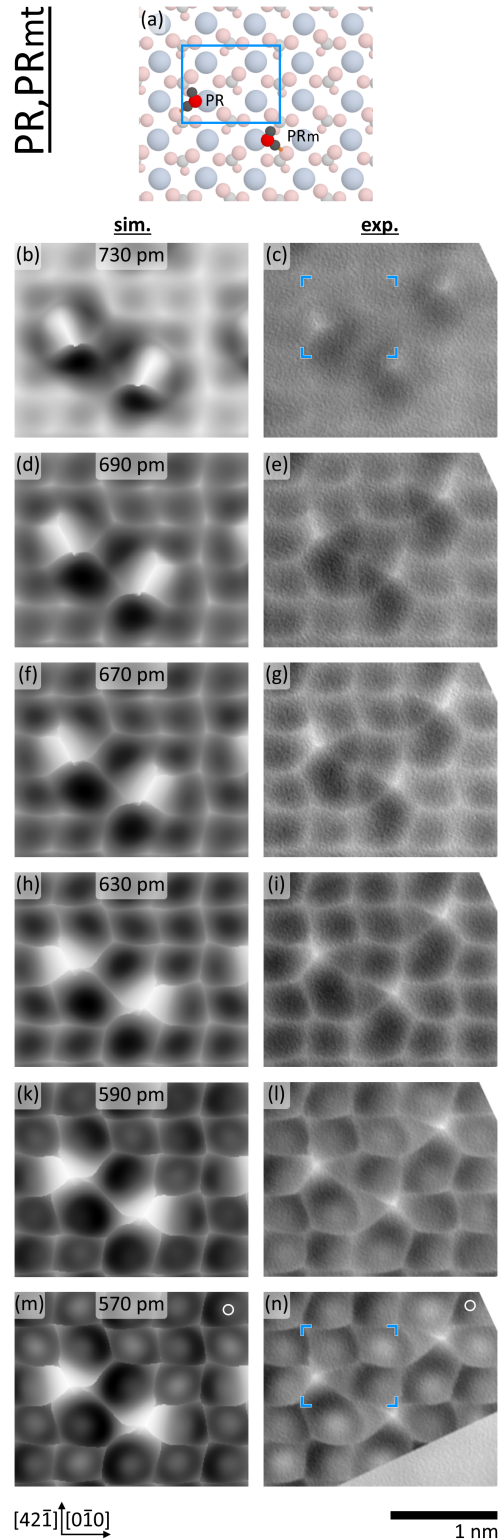


FIG. S8. PR,PR_{mt} dimer: (a) DFT model as well as (b,d,f,h,k,m) simulated and (c,e,g,i,l,n) experimental constant-height frequency shift images.

III. CONSTANT-HEIGHT IMAGING OF A QS-WATER ROW STRUCTURE

Fig. S9 presents an experimental image series (right column) complemented by the simulated data (left column) for a QS water row.

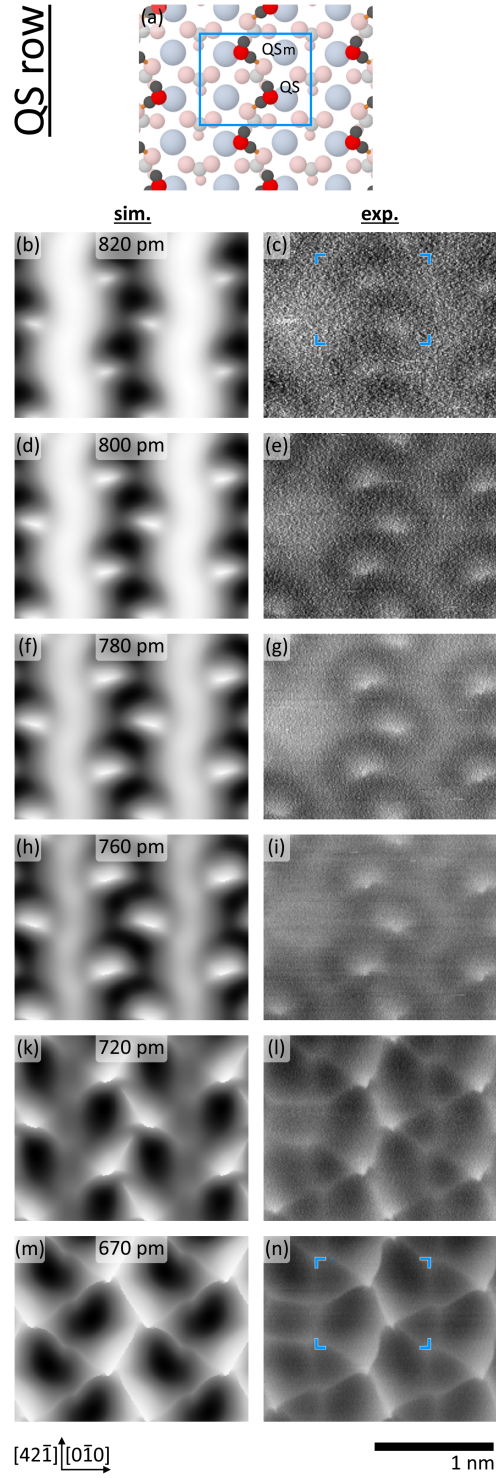


FIG. S9. QS water row: (a) DFT model as well as (b,d,f,h,k,m) simulated and (c,e,g,i,l,n) experimental constant-height frequency shift images. (DFT model atomic coordinates from Ref. [1])

IV. LINE PROFILES

Line profiles extracted from experimental and simulated data at different heights are compared in Fig. S10 and Fig. S11 for the QS and PR water monomers, respectively. An overall good match is found, in particular the shoulder on the right side of the maximum peak reproduces in both experimental and simulated data (marked by arrows). The different slope of this shoulder is explained by the different environment of the calcite lattice, i.e. the presence of either a reconstructed or an unreconstructed CO_3 group row nearby the water molecule. Note that the absolute values, the vertical contrast, and the sharpness of the water pattern are not expected to precisely reproduce for following two reasons: First, the PPM model does not include the mesoscopic and macroscopic tip body. Thus, the long-range background forces are missing. To consider these force components, we visually shifted each curve by multiples of -0.5 Hz in Figures S10(d) and S11(d). Second, the surface geometry is fixed in the PPM simulations. As the surface atoms are expected to physically relax in presence of the repulsive interaction with the CO tip, the vertical forces will be overestimated in the simulations due to an apparent stronger repulsion.

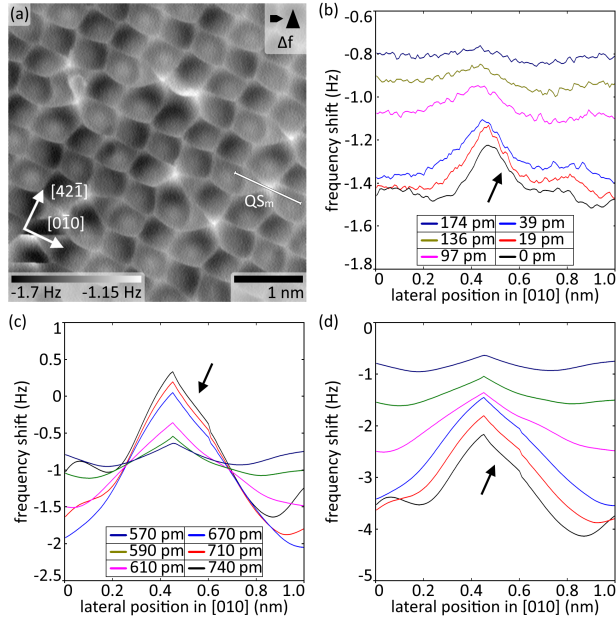


FIG. S10. Lineprofiles across a QS water monomer extracted at different tip-sample heights at the lateral position as marked in the AFM image (a). Line profiles from (b) experimental data, (c) PPM simulation, and (d) PPM simulations. Line profiles are offset by multiples of -0.5 Hz per profile in (d).

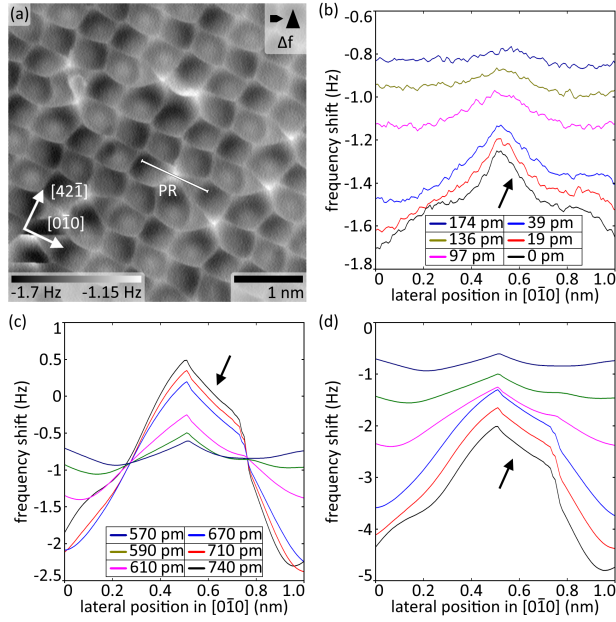


FIG. S11. Lineprofiles across a PR water monomer extracted at different tip-sample heights at the lateral position as marked in the AFM image (a). Line profiles from (b) experimental data, (c) PPM simulation, and (d) PPM simulations. Line profiles are offset by multiples of -0.5 Hz per profile in (d).

V. ATOMIC SHIFTS

Atomic shifts are calculated from comparing the coordinates of the calcite top layer atoms and water molecules between two selected DFT geometries. One calcium atom at large distance from the water molecules is chosen as reference for the origin (note the periodic boundary conditions that limit the choice). By definition, the shift of this calcium atom is zero.

Fig. S12 presents the atomic shifts determined for the top calcite layer when comparing the pristine calcite(104)–(2×1) surface with the QS and PR water/calcite models. Absolute shifts (norm of the shift vector) of more than 5 pm are included as numbers in Fig. S12(a,c) (in units of 1 pm) with the lateral directions indicated by arrows (arrow length increased by a factor of three). The vertical shifts are encoded via a red-black-blue colormap that is used for coloring the arrows. The shifts indicate the change from the pristine surface to the water/calcite system. Therefore, the solid circles represent the calcite(104) – (2 × 1) model and the position of the water molecules are indicated as half-transparent circles. The absolute shift distance for each atom are shown in Fig. S12(b,d). Clearly, shifts of up to 60 pm are observed for the PR/calcite water structure, while only very few atoms in the QS/water model move by more than 5 pm.

This analysis reveals that there are significant shifts present at the calcium atoms and carbonate groups nearby the water molecule, in particular for the PR/calcite water model. The relevant atoms and groups are marked by dashed green circles in Fig. S12. Most interesting is the finding that the two calcium atoms surrounding the bulk-like (S) carbonate group row shift by 19 pm and 6 pm that in turn lead to significant shifts of up to 24 pm of the S carbonate group atoms (marked by green dashed circle in Fig. S12). Thus, we conclude that the adsorption of P water has an effect on the neighboring adsorption site besides reorienting the direct adjacent carbonate group. A smaller, stronger localized, but still measurable effect is also present for the Q water/calcite system as marked in Fig. S12(a).

When performing the same analysis for the QS,PRt dimer, namely when comparing the dimer geometry to the geometries of the QS/calcite(104)–(2×1) and PR/calcite(104)–(2×1) single water models, the competing influence on the surface atoms exerted by the two water molecules becomes apparent. Results are shown in Fig. S13, using the identical layout and marking as explained before. The comparison with the QS single water model uncovers shifts

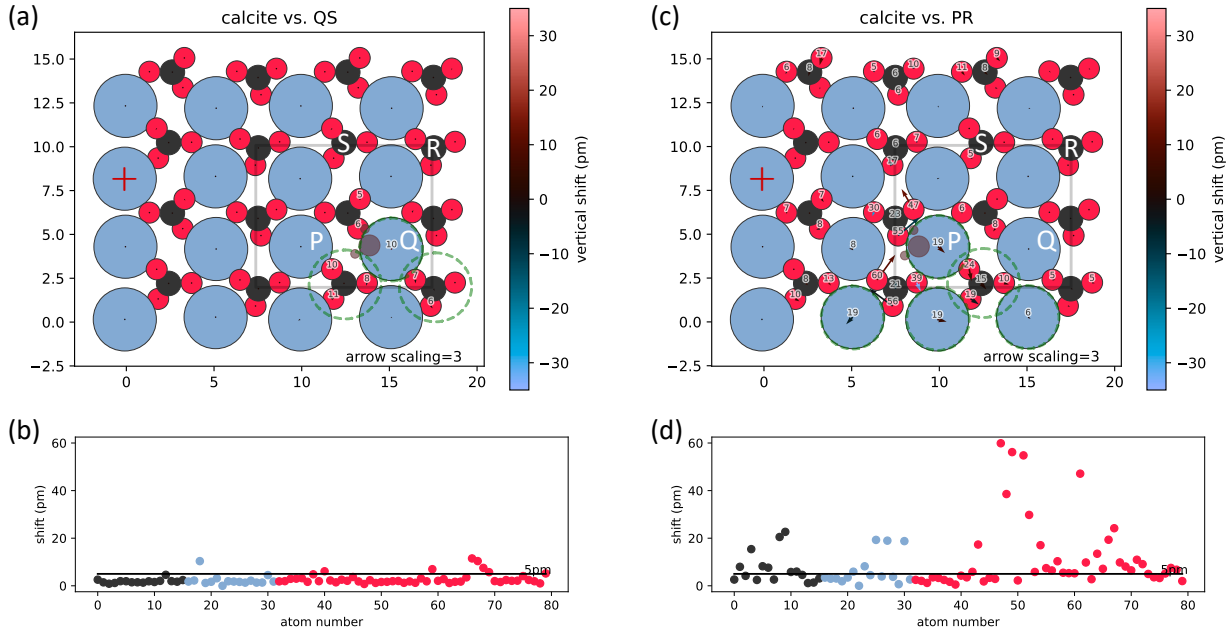


FIG. S12. Atomic shifts analysed for the (a,b) QS water/calcite(104) – (2 × 1) and the (c,d) PR water/calcite(104) – (2 × 1) systems. (a,c) Sketch of the top layer atomic model. Shifts above 5 pm are included as numbers, lateral shift directions visualised by arrows (arrows enlarged by a factor of 3), color of the arrows correspond to the vertical shift (see color bars right of the images). Lateral dimensions are in 1 Å, atomic shifts in 1 pm. Reference atom marked by a red cross. (b,d) Absolute shifts for each atom of the top layer. 5 pm threshold included as a black line.

mainly of the calcium atoms located below the two water molecules as well as the adjacent carbonate groups, see green-dashed circles in Fig. S13(a). Shifts are more pronounced when comparing the dimer structure to the single PR water geometry as shown in Fig. S13(c) with major effects on one calcium ion and three adjacent carbonate groups as marked by green dashed circles in Fig. S13(c).

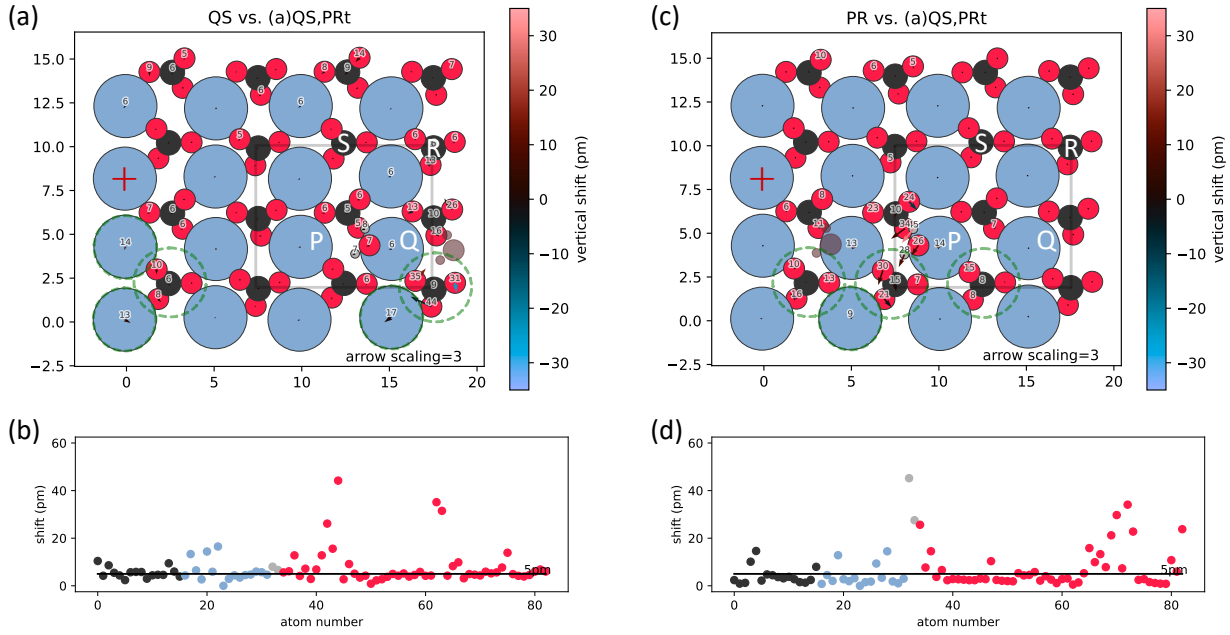


FIG. S13. Atomic shifts analysed for the QS,PRt water dimer/calcite(104) – (2 × 1) structure, comparing the dimer geometry to (a,b) the QS water/calcite(104) – (2 × 1) and the (c,d) PR water/calcite(104) – (2 × 1) geometries. (a,c) Sketch of the top layer atomic model. Shifts above 5 pm are included as numbers, lateral shift directions visualised by arrows (arrows enlarged by a factor of 3), color of the arrows correspond to the vertical shift (see color bars right of the images). Lateral dimensions are in 1 Å, atomic shifts in 1 pm. Reference atom marked by a red cross. (b,d) Absolute shifts for each atom of the top layer. 5 pm threshold included as a black line.

-
- [1] J. Hegemann, S. Aeschlimann, T. Dickbreder, Y. S. Ranawat, R. Bechstein, A. Kühnle, A. S. Foster, and P. Rahe, Water adsorption lifts the (2×1) reconstruction of calcite(104), *Physical Chemistry Chemical Physics* **26**, 21365 (2024).